TURBULENCE STRUCTURE IN A STRATIFIED BOUNDARY LAYER UNDER STABLE CONDITIONS

YUJI OHYA
Research Institute for Applied Mechanics, Kyushu University, Kasuga 816, Japan
DAVID E. NEFF and ROBERT N. MERONEY
Department of Civil Engineering, Colorado State University, Fort Collins, Colorado 80523, U.S.A.

(Received in final form 5 November, 1996)

Abstract. Turbulence structure in stably stratified boundary layers is experimentally investigated by using a thermally stratified wind tunnel. A stably stratified flow is created by heating the wind tunnel airflow to a temperature of about 50 °C and by cooling the test-section floor to a surface temperature of about 3 °C. In order to study the effect of buoyancy on turbulent boundary layers for a wide range of stability, the velocity and temperature fluctuations are measured simultaneously at a downwind position of 23.5 m from the tunnel entrance, where the boundary layer is fully developed. The Reynolds number, Re_δ, ranges from 3.14×10^4 to 1.27×10^5, and the bulk Richardson number, Ri_δ, ranges from 0 to 1.33. Stable stratification rapidly suppresses the fluctuations of streamwise velocity and temperature as well as the vertical velocity fluctuation. Momentum and heat fluxes are also significantly decreased with increasing stability and become nearly zero in the lowest part of the boundary layer with strong stability. The vertical profiles of turbulence quantities exhibit different behaviour in three distinct stability regimes, the neutral flows, the stratified flows with weak stability (Ri_δ = 0.12, 0.20) and those with strong stability (Ri_δ = 0.39, 0.47, 1.33). Of these, the two regimes of stratified flows clearly show different vertical profiles of the local gradient Richardson number Ri, separated by the critical Richardson number Ri_{cr} of about 0.25. Moreover, turbulence quantities in stable conditions are well correlated with Ri.

Key words: Wind tunnel experiment, Thermal stratification, Stable boundary layer, Turbulence structure, Buoyancy effect

List of Symbols

f	frequency
g	acceleration due to gravity
K	yaw factor of hot-film
K_m	eddy exchange coefficient of momentum ($= -\overline{uw}/(\partial U/\partial z)$)
K_h	eddy exchange coefficient of heat ($= -\overline{u\theta}/(\partial \Theta/\partial z)$)
k	wavenumber ($= 2\pi f/U$)
L	Obukhov length ($= -u_*^3\Theta/\kappa g Q_s$)
Q_s	surface kinematic heat flux ($= (\overline{w\theta})_s - \alpha(\partial\Theta/\partial z)_s$)
Re_δ	Reynolds number based on δ ($= U_\infty \delta/\nu$)
Ri_δ	bulk Richardson number ($= g\delta\Delta\Theta/\Theta_0 U_\infty^2$)
Ri	local gradient Richardson number ($= (g/\Theta)\cdot(\partial\Theta/\partial z)/(\partial U/\partial z)^2$)

Boundary-Layer Meteorology **83:** 139–161, 1997.

U_∞	ambient velocity
U, W	mean velocity components in x, z direction
u, w	fluctuating velocity components in x, z direction
u_*	friction velocity $(= (\tau_s/\rho)^{1/2})$
u'	r.m.s. value of u fluctuation $(= \sqrt{\overline{u^2}})$
$\overline{uw}$	vertical turbulent momentum flux
$\overline{u\theta}$	horizontal turbulent heat flux
$\overline{w\theta}$	vertical turbulent heat flux
w'	r.m.s. value of w fluctuation $(= \sqrt{\overline{w^2}})$
α	coefficient of thermal diffusivity
δ	momentum boundary-layer thickness
δ_θ	thermal boundary-layer thickness
κ	Karman's constant (= 0.4)
μ	coefficient of dynamic viscosity
ν	coefficient of kinematic viscosity
Θ	mean temperature
Θ_∞	temperature of ambient air
Θ_s	temperature of cooled floor
$\Delta\Theta$	temperature difference $(= \Theta_\infty - \Theta_s)$
Θ_0	average absolute temperature in boundary layer
θ	fluctuating temperature
θ_*	friction temperature $(= -Q_s/u_*)$
θ'	r.m.s. value of θ-fluctuation $(= \sqrt{\overline{\theta^2}})$
ρ	mean mass density of the air
τ_s	surface shear stress $(= -\rho(\overline{uw})_s + \mu(\partial U/\partial z)_s)$

1. Introduction

Stratified flows in the atmospheric boundary layer, depending on the stability, can be classified into three characteristic regimes: the mixed layers which are convectively driven, unstable turbulent flows in the daytime, the nocturnal stable boundary layers that are often accompanied by weak and sporadic turbulence, and the statically neutral flows. These boundary layer flows show greatly different turbulence structure and transport processes from each other.

The atmospheric boundary layer under stable stratification is especially difficult to describe and model (Stull, 1988). The balance between mechanical generation of turbulence and damping by stability varies from case to case, creating stable boundary layers that range very widely from well mixed to non turbulent. Sometimes the turbulence in stable boundary layers is intermittent and patchy, allowing the upper portions of the boundary layer to decouple from surface forcings.

Observational studies of stable atmospheric boundary layers have been less frequently reported compared with mixed layers, because of the difficulties and complexity associated with unsteadiness, non-uniformity and sensitivity to terrain

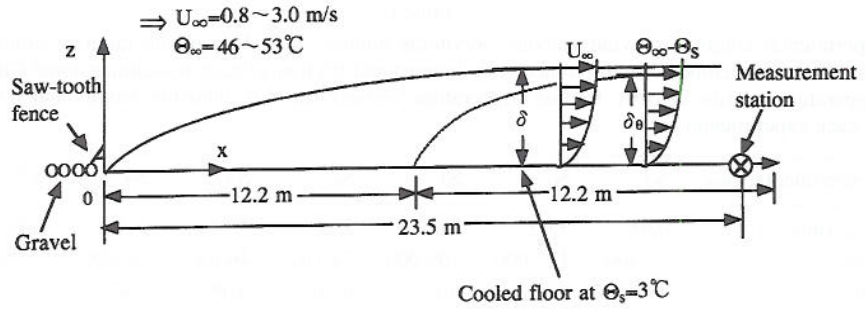

Figure 1. Experimental arrangement.

slope of the nocturnal boundary layer. Nonetheless, there have been sufficient results to identify various significant characteristics from such observations. For convenience, we define the overall stability of the whole boundary layer through a bulk Richardson number, Ri_δ, based on the height at which the wind speed reaches a maximum, and the velocity and temperature differences over the height. According to this definition, the observational studies of Caughey et al. (1979) ($Ri_\delta \sim 0.14$), and Garratt (1982) and Nieuwstadt (1984) ($Ri_\delta \sim 0.16$) are related to stratified flows with weak or moderate stability, where turbulence is dominant. They have reported vertical profiles of turbulent variances and fluxes of wind velocity and temperature fluctuations. For stratified flows with strong stability, studies include Yamamoto et al. (1979), Mahrt et al. (1979) ($Ri_\delta \sim 0.26 - 0.34$), Finnigan and Einaudi (1981) and Andre and Mahrt (1982) ($Ri_\delta \sim 0.5$). Finnigan and Einaudi (1981) have demonstrated the respective contribution of internal gravity waves and turbulence to the vertical distributions of turbulent variances and fluxes, which are quite different from those for neutrally and weakly stable flows. For very strong stable flows, the occurrence of internal gravity waves has been clearly shown by Kondo et al. (1978), Finnigan et al. (1984), Hunt et al. (1985) and Mahrt (1985). Thus, a variety of types of turbulence can occur in the stable boundary layer.

Since observational studies are intrinsically limited, the feasibility of laboratory simulation of stratified flows has led to their study in specially designed wind and water tunnels (Meroney, 1990). However, only a few laboratory experiments have been reported for stably stratified boundary layers, including Arya and Plate (1969), Nicholl (1970), Arya (1975), Piat and Hopfinger (1981), Ogawa et al. (1982, 1985) and others. Of these experimental works, Arya (1975) ($Ri_\delta < 0.1$) and Ogawa et al. (1985) ($Ri_\delta < 0.25$) have performed detailed investigations of the effect of buoyancy on turbulent boundary layers in a thermally stratified wind tunnel. They have shown that under stable conditions turbulence becomes rapidly suppressed with increasing stability as more and more energy has to be expended in overcoming buoyancy forces. Komori et al. (1983) carried out a similar experiment using an open water-channel flow ($Ri_\delta < 0.27$). They have shown that turbulence quantities in stable conditions are well correlated with the local gradient Richardson number

Table I

Experimental conditions: wind velocity, Reynolds number, bulk Richardson number, boundary layer thickness, temperature difference, non-dimensional friction velocity,non-dimensional friction temperature, friction velocity, friction temperature, vertical heat flux, Obukhov length, and symbol for each experimental case

Experimental case	N1	N2	S1	S2	S3	S4	S5
U_∞ (m s^{-1})	0.98	3.05	2.95	2.16	1.44	1.30	0.82
Re_δ	31 400	127 000	109 000	74 100	46 000	42 000	31 500
Ri_δ	0	0	0.12	0.20	0.39	0.47	1.33
$\delta(\fallingdotseq \delta_\theta)$ (m)	0.5	0.65	0.65	0.6	0.55	0.55	0.65
$\Delta\Theta$ (°C)	0	0	49.6	49.3	46.7	45.6	43.6
u_*/U_∞	0.040	0.043	0.026	0.022	0.018	0.017	0.016
$\theta_*/\Delta\Theta$	0	0	0.025	0.027	0.027	0.030	0.028
u_* (m s^{-1})	0.039	0.13	0.078	0.047	0.027	0.022	0.013
θ_* (°C)	0	0	1.25	1.32	1.25	1.38	1.21
Q_s (m s^{-1} °C)	0	0	−0.097	−0.062	−0.033	−0.031	−0.016
L (m)	–	–	0.367	0.125	–	–	–
Symbol	—■—	—●—	—◇—	—△—	—▽—	—□—	—○—

Ri . Most of those laboratory studies, however, have focused on the stratified flows with weak stability condition ($Ri_\delta < 0.25$). Therefore, the turbulence structure and transport processes in strongly stable boundary layers in a range of $Ri_\delta > 0.25$ remain unclear.

The purpose of the present study is to clarify the buoyancy effects on the turbulence structure for a wide range of stability (up to Ri_δ =1.33) in stably stratified boundary layers in a specially designed wind tunnel. The present flow configuration is the same as used in the Arya's experimental work (1975), where thermally stratified boundary layers under stable conditions are created by heating the tunnel airflow and by cooling the test-section floor. The velocity and temperature fluctuations are measured simultaneously at a downwind position, where the boundary layer is fully developed over a long distance.

2. Experimental Arrangement

2.1. Wind Tunnel

Experiments were performed in the meteorological wind tunnel (Plate and Cermak, 1963) at Colorado State University. The closed-circuit tunnel has a 1.8 × 1.8 × 28 m long test section and is equipped with two independent temperature controlling systems. The air-conditioning system allows the ambient air temperature to be maintained anywhere between 5 and 65 °C. Over the last 12.2 m of the test section,

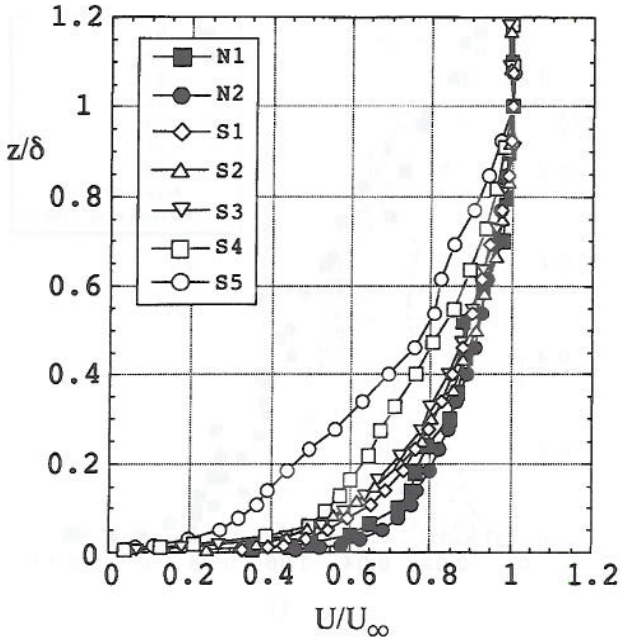

Figure 2a. Vertical profiles of the mean streamwise velocity U.

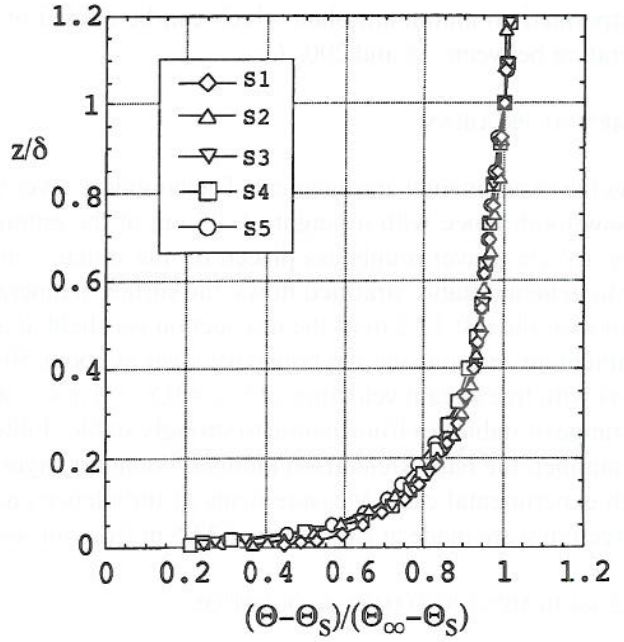

Figure 2b. Vertical profiles of the mean temperature Θ.

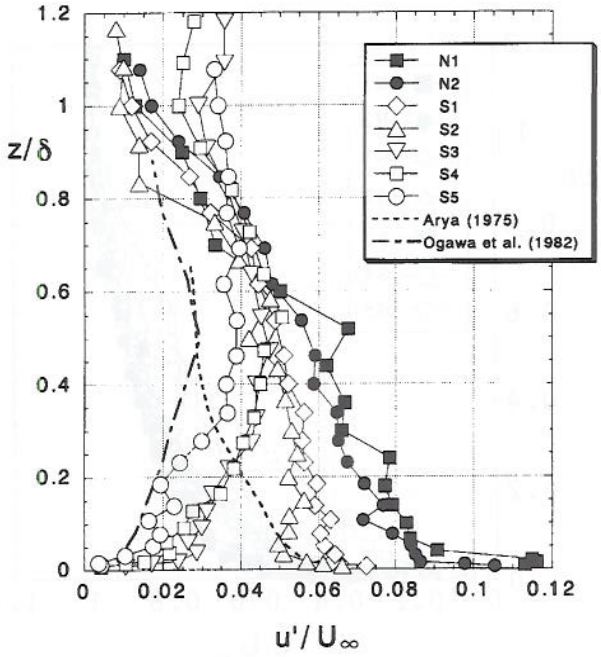

Figure 3a. Vertical profiles of the turbulent intensities (r.m.s. values), u-component velocity u'; dashed line, Arya (1975), $Ri_\delta = 0.1$; dash/dotted line, Ogawa et al. (1982), $Ri_\delta = 0.57$.

the floor incorporated an aluminum plate which can be cooled or heated to any desired temperature between −5 and 200 °C.

2.2. Experimental Program

Figure 1 shows the experimental arrangement. The boundary layer was artificially tripped by a saw-tooth fence with a height of 3.5 cm at the entrance of the test section and by 1.2 cm gravel roughness placed on the initial 2 m length of the floor. In order to generate stably stratified flows, the surface temperature Θ_s of the aluminum floor over the last 12.2 m of the test section was held at about 3 °C and that of the ambient air Θ_∞ outside the boundary layer at about 50 °C. Turbulent boundary layers with free stream velocities of $U_\infty = 0.8$–3.0 m s^{-1} were produced. These cover a range of stabilities from neutral to strongly stable. Table I summarizes the Reynolds number, the bulk Richardson number, boundary layer thickness and others for each experimental case. Measurements of turbulence characteristics in the vertical direction were made at a distance of 23.5 m from the saw-tooth fence.

2.3. Flow Measurement and Data Acquisition

The free stream velocities, U_∞, outside the boundary layers were monitored with a standard Pitot-static tube in conjunction with an electronic manometer. Floor sur-

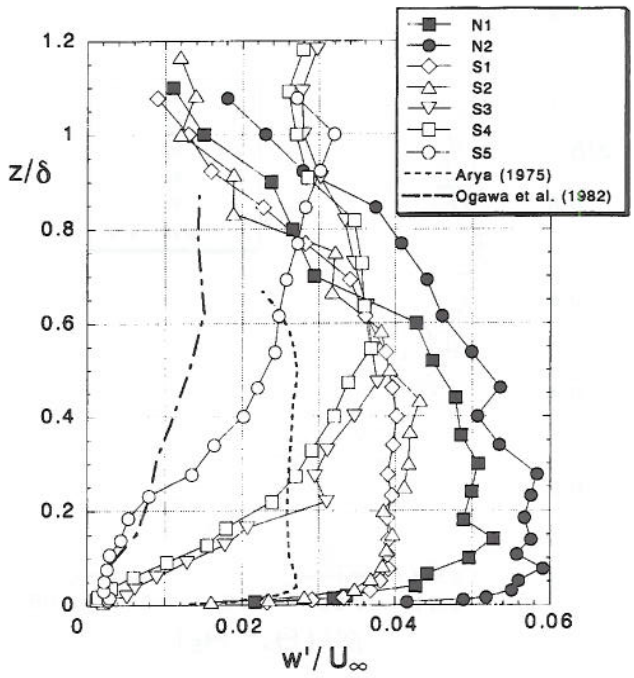

Figure 3b. Vertical profiles of the turbulent intensities (r.m.s. values), w-component velocity w'; dashed line, Arya (1975), $\mathrm{Ri}_\delta = 0.1$; dash/dotted line, Ogawa et al. (1982), $\mathrm{Ri}_\delta = 0.57$.

face temperatures, Θ_s, were measured with a surface thermocouple and monitored with a set of thermocouples embedded in the aluminum plate at 30 cm intervals along the center-line.

Simultaneous measurements of streamwise and vertical velocities, u and w, and of fluctuating temperature, θ, were obtained using thermal anemometry, but adjusting for the large temperature variations in interpreting the sensor response. The sensors consist of an x-type hot-film probe for velocity and a thin thermocouple probe of 0.025 mm diameter for temperature with a separation of 1 mm. The output voltage, E, of a constant-temperature anemometer is represented at a sensor temperature, Θ_w (given at 250 °C), air temperature, Θ, and flow speed, U, by

$$E^2 = (\mathrm{A} + \mathrm{B} \cdot U_{\mathrm{eff}}^{\mathrm{m}})(\Theta_w - \Theta),$$

where $U_{\mathrm{eff}} = U(\cos^2\phi + K^2 \sin^2\phi)^{1/2}$.

Here, A, B and m are constants given by a calibration curve for an ambient temperature. K is the yaw angle coefficient of x-type hot-film probe and ϕ is the hot-film angle to the direction of the mean flow. Thus, cross-film data were corrected point by point for temperature fluctuation deviations using the above relation. Calibration was carried out in a special calibration unit with a nozzle and mass-flow meter. The velocity at the nozzle exit is provided by the mass-flow meter.

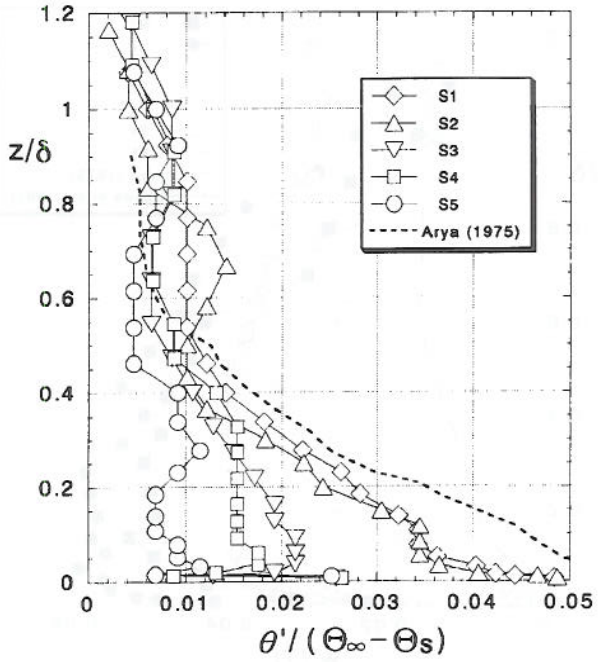

Figure 3c. Vertical profiles of the turbulent intensities (r.m.s. values), temperature θ'; dashed line, Arya (1975), $Ri_\delta = 0.1$.

A calibration curve for each experimental case was obtained for a temperature at a middle value in the boundary layer to reduce the error due to temperature difference. The calibration unit covers a range of wind velocity of $U_\infty = 0 - 4.0$ m s^{-1} and can easily determine the yaw angle coefficient K of cross-film probe by rotating the nozzle of the unit. Calibration for temperature was made with a thermocouple calibrator. A traversing system was used for profile measurements.

For data acquisition, the three channels of amplified signals (cross-film and temperature probe) were digitized by an A/D converter (12 bit) at a sampling frequency of 300 Hz, after a low-pass filter of 150 Hz. The data were then analysed on a computer. The number of sampling data for each component of u, w, and θ for each measurement point was 20480, i.e., the sampling period is about 70 s.

3. Results

3.1. Experimental flow conditions

Table I shows the flow conditions for each experimental case (N1-S5), such as the wind velocity, U_∞, Reynolds number , Re_δ, bulk Richardson number, Ri_δ, and so on. The streamwise homogeneity, in the sense that velocity and temperature

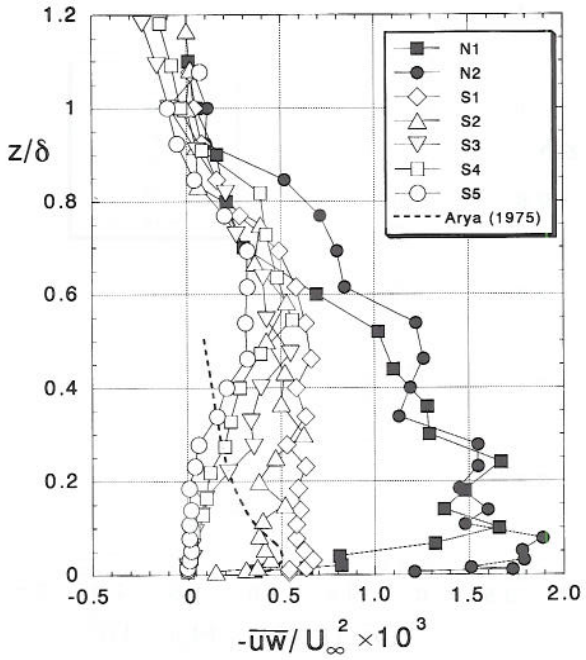

Figure 4a. Vertical profiles of the turbulent fluxes, momentum flux $-\overline{uw}$; dashed line, Arya (1975), $Ri_\delta = 0.1$.

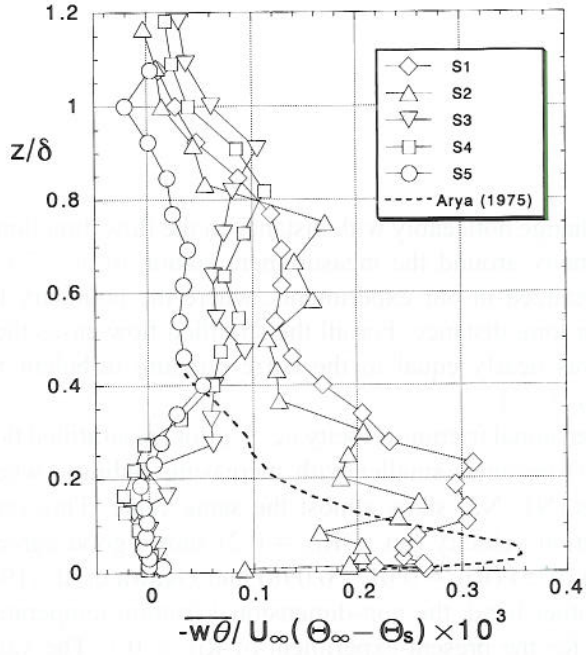

Figure 4b. Vertical profiles of the turbulent fluxes, vertical heat flux $-\overline{w\theta}$; dashed line, Arya (1975), $Ri_\delta = 0.1$.

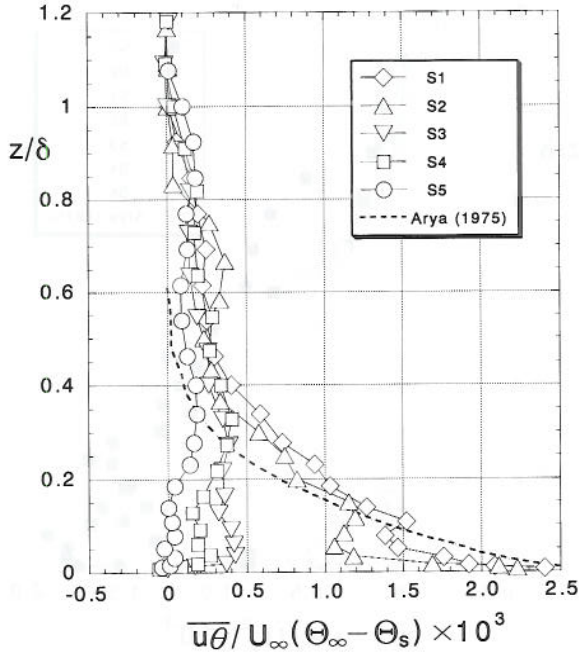

Figure 4c. Vertical profiles of the turbulent fluxes, horizontal heat flux $\overline{u\theta}$; dashed line, Arya (1975), $\mathrm{Ri}_\delta = 0.1$.

profiles do not change noticeably with distance in the flow direction and the cross-section homogeneity around the measurement station of x = 23.5 m, has been approximately realized in our experiments, where the boundary layer was fully developed over a long distance. For all the stratified flow cases the thermal-layer thickness, δ_θ, was nearly equal to the corresponding turbulent boundary-layer thickness, i.e., $\delta_\theta/\delta \sim 1$.

The non-dimensional friction velocity u_*/U_∞ for the stratified flow cases (especially for S1–S3) becomes smaller with increasing stability, whereas those for the neutral cases (N1, N2) show almost the same value. This variation of non-dimensional friction velocity (up to Ri_δ = 0.2) shows good agreement with the results of Arya (1975) (Ri_δ = 0.01 – 0.098) and Ogawa et al. (1985) (Ri_δ = 0 – 0.248). On the other hand, the non-dimensional friction temperature, $\theta_*/\Delta\Theta$, is almost constant for the present experiment of $\mathrm{Ri}_\delta > 0.1$. The values of u_*/U_∞ and $\theta_*/\Delta\Theta$ for the strong stability cases (S4, S5) are similar to those reported by Ogawa et al. (1982) (Ri_δ = 0.57, u_*/U_∞ = 0.021 and $\theta_*/\Delta\Theta$ = 0.03).

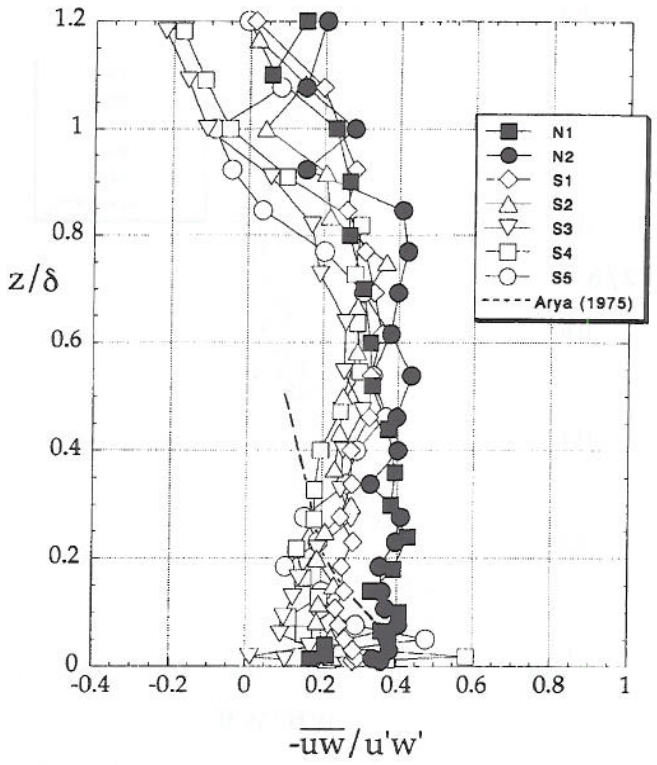

Figure 5a. Vertical profiles of the correlation coefficients, momentum flux $-\overline{uw}/u'w'$; dashed line, Arya (1975), $\mathrm{Ri}_\delta = 0.1$.

3.2. VERTICAL PROFILES OF MEAN AND TURBULENT QUANTITIES

The vertical profiles in Figures 2–4 are normalized by the ambient velocity U_∞ and temperature difference $\Delta\Theta$ $(= \Theta_\infty - \Theta_s)$ and are shown with the normalized height z/δ.

The turbulence characteristics of stratified flows are generally dependent on both Re_δ and Ri_δ. In order to investigate the effect of the Reynolds number in our experiment, we have included the measurements of two neutral flow cases (N1, N2), the Reynolds numbers of which cover those for all the stratified flow cases. The results of cases (N1, N2), as displayed in Figures 2–5, show similar profiles to each other without indicating any significant effect of Reynolds number. In this way, any variation with Reynolds number is expected to be eliminated, especially within the narrow range of Reynolds number in our experiments.

Figures 2a, b show the mean velocity and temperature profiles in the vertical direction. Large variations in the 'defect' profiles in Figure 2a are mainly due to changes in thermal stratification. For the strongest stability case S5, the profile shows a laminar flow type. In Figure 2b, all the distributions of mean temperature

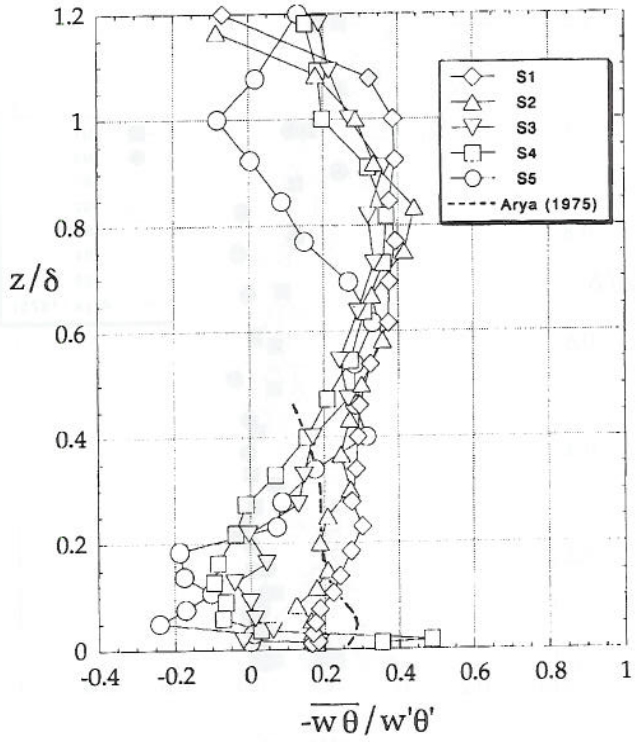

Figure 5b. Vertical profiles of the correlation coefficients, vertical heat flux $-\overline{w\theta}/w'\theta'$; dashed line, Arya (1975), $Ri_\delta = 0.1$.

show almost the same profile except for a narrow region in the lowest part of the boundary layer.

Figures 3a–c show the vertical profiles of normalized r.m.s. fluctuations of the u and w-component, and temperature θ. These profiles display strong differences in the lower half depth of the boundary layer. Buoyancy forces in stratified flows extract energy directly from the vertical component w of the velocity, thereby reducing $\overline{w^2}$, as shown in Figure 3b, and subsequently $-\overline{uw}$ (see Figure 4a, discussed later). The intensities of u' and θ' are also reduced remarkably with increasing stability, because energies associated with different velocity components are redistributed according to their kinetic energy budget equations. For the weak stability cases (S1, S2: Ri_δ= 0.12, 0.2) in Figure 3, the vertical profiles of u', w' and θ' almost agree with those obtained in wind-tunnel experiments by Arya (1975), where Ri_δ is around 0.1, although the Arya's values of u' and w' are rather smaller than those of our cases S1 and S2. Moreover, the u', w' and θ' profiles of the weak stability cases (S1, S2) are similar to the observational results from Caughey et al. (1979) rather than those from Nieuwstadt (1984), for which the θ' variation shows a rapid decrease with height. For the strong stability cases (S3, S4 and S5: Ri_δ = 0.39, 0.47, 1.33), the vertical profiles of u' and w' are similar to the results obtained

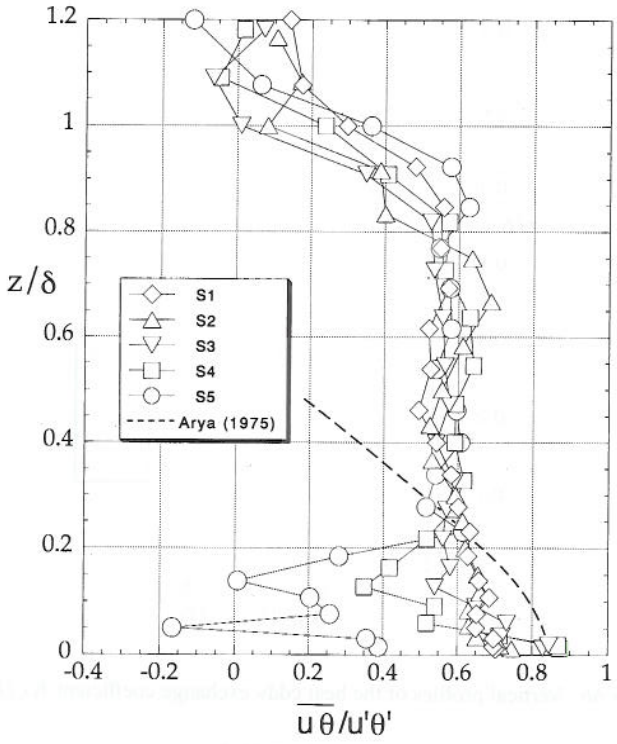

Figure 5c. Vertical profiles of the correlation coefficients, horizontal heat flux $\overline{u\theta}/u'\theta'$; dashed line, Arya (1975), $Ri_\delta = 0.1$.

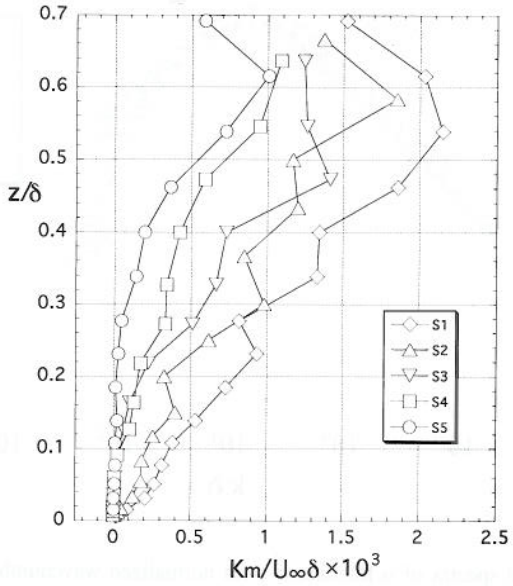

Figure 6a. Vertical profiles of the momentum eddy exchange coefficient $K_m/U_\infty\delta$.

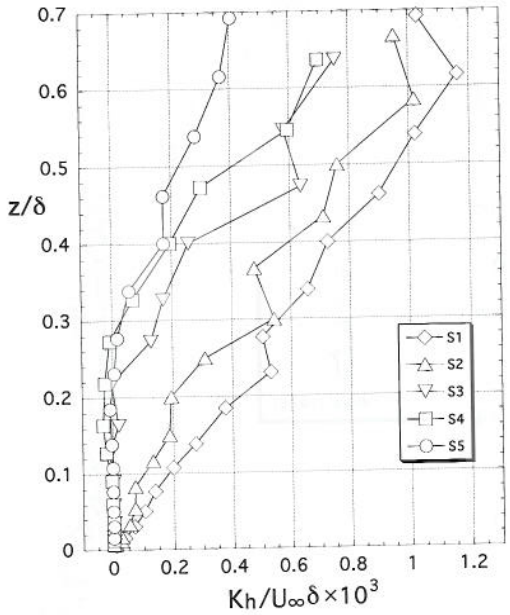

Figure 6b. Vertical profiles of the heat eddy exchange coefficient $K_h/U_\infty\delta$.

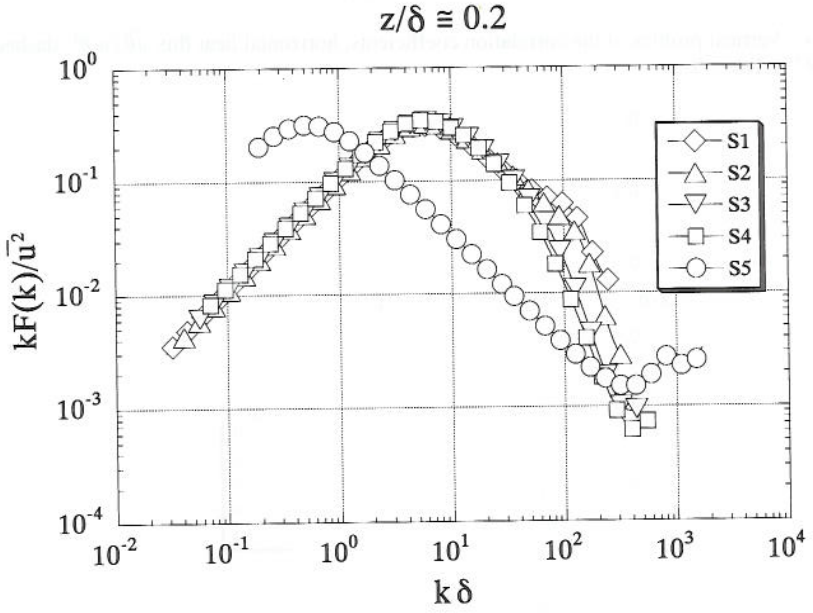

Figure 7a. Normalized spectra of u fluctuation with normalized wavenumber $k\delta$ for all stratified flows stratified flow cases (S1–S5) at around $z/\delta = 0.2$.

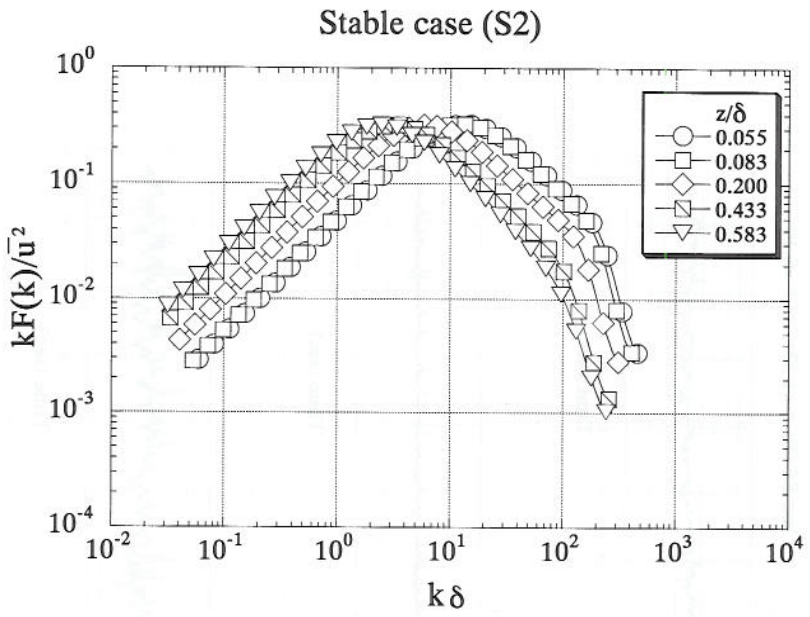

Figure 7b. u spectra at five heights of z/δ for the case S2 with weak stability ($Ri_\delta = 0.2$).

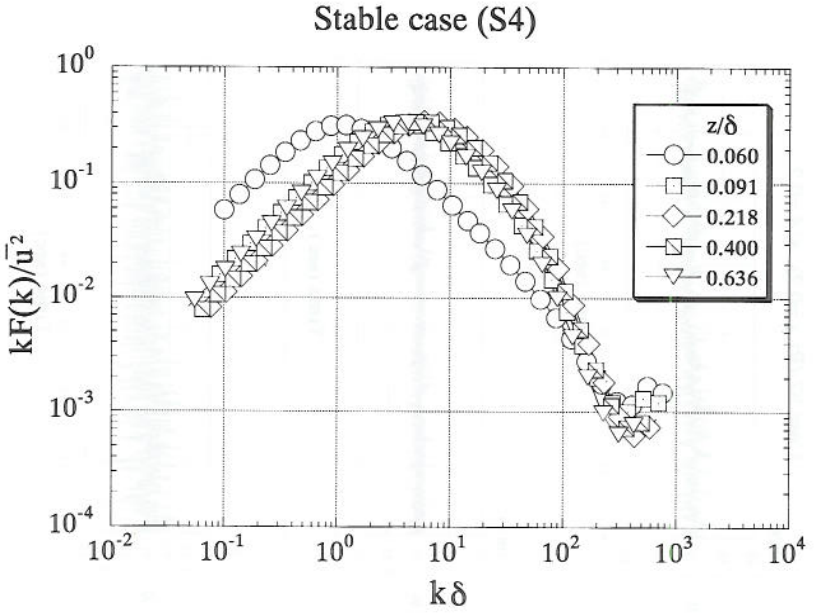

Figure 7c. u spectra at five heights of z/δ for the case S4 with strong stability ($Ri_\delta = 0.47$).

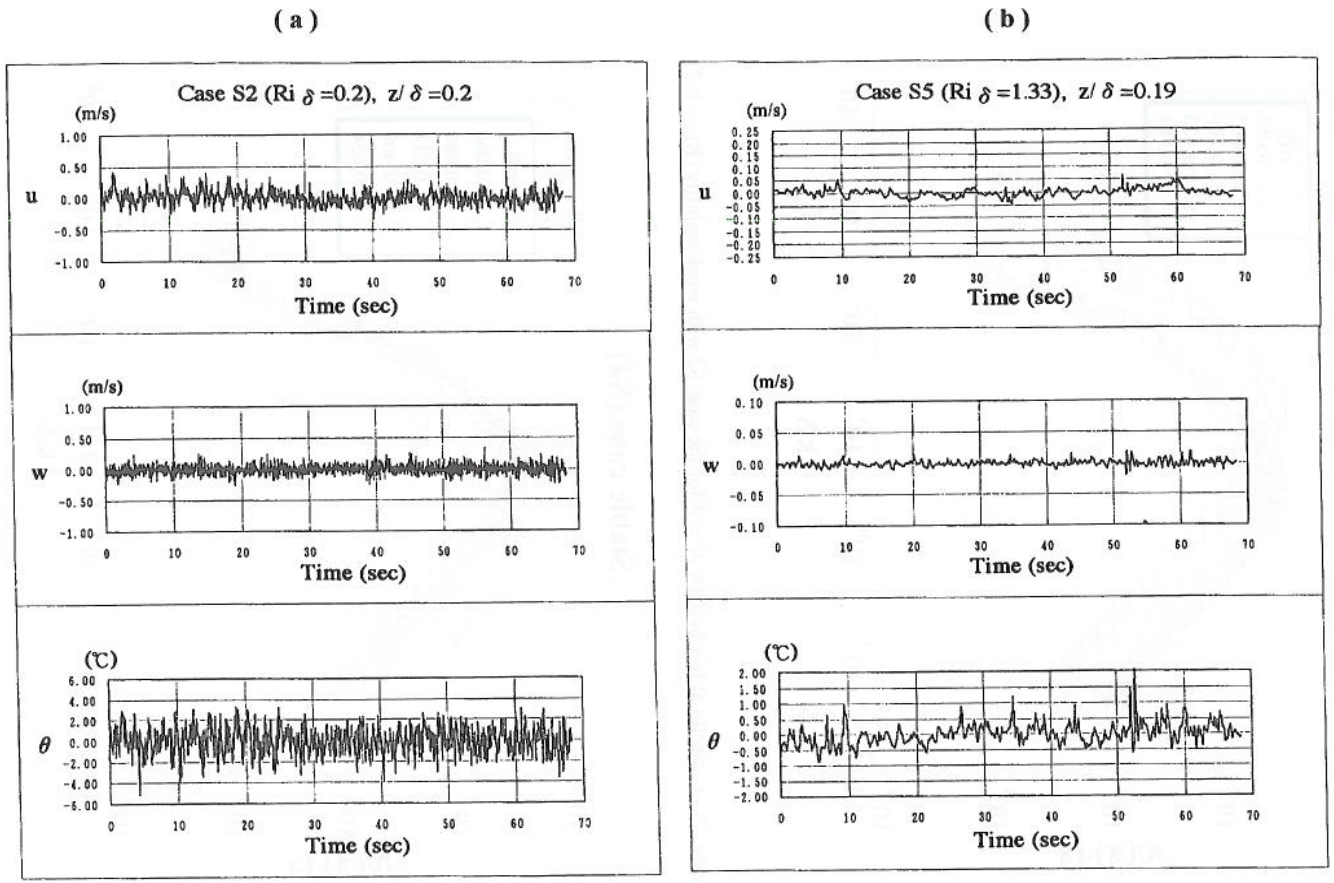

Figure 8. Time series of u, w and θ fluctuations measured at around $z/\delta = 0.2$, note that the amplitude scales of (a) are different from those of (b). (a) Case S2 with weak stability ($Ri_\delta = 0.2$); (b) Case S5 with strong stability ($Ri_\delta = 1.33$).

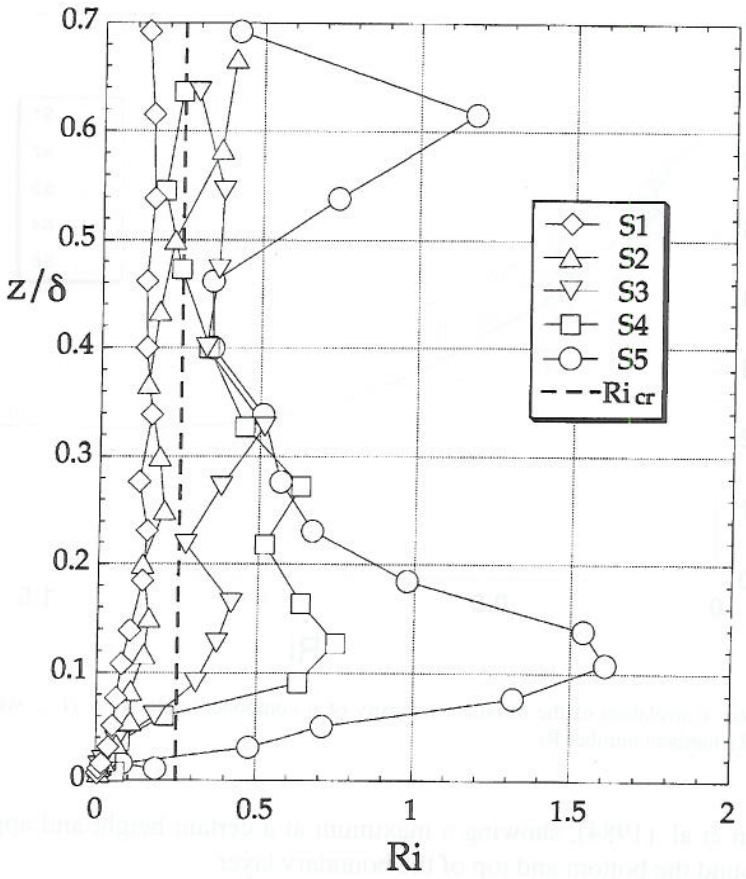

Figure 9. Vertical profiles of the local gradient Richardson number Ri.

in a wind-tunnel experiment (Ri_δ = 0.57) by Ogawa et al. (1982), although they are rather small. The feature of those profiles is that the intensities of u and w fluctuations approach zero as z/δ decreases from the middle of the boundary layer to the bottom. We can find similar profiles of $\overline{u^2}$ and $\overline{w^2}$ in the observational studies of Finnigan and Einaudi (1981) and that of $\overline{w^2}$ in Mahrt (1985).

Figure 4a shows the vertical profiles of vertical turbulent momentum flux $\overline{uw}$. For the stratified flow cases (S1–S5), $\overline{uw}$ values are remarkably decreased for $z/\delta < 0.6$, compared with those for the neutral flow cases (N1, N2). Furthermore, for the strong stability cases (S3–S5), $\overline{uw}$ values are almost zero for $z/\delta < 0.2$. Thus, the profiles exhibit different behaviour for the three distinct stratification regimes. The tendency for the turbulence profiles to separate into three sets is also seen in Figure 3. For the weak stability group (S1, S2), the profiles of $\overline{uw}$ are similar to the observational results by Caughey et al. (1979) and Nieuwstadt (1984). For the strong stability group (S3–S5), the profiles of $\overline{uw}$ are similar to the results from observational studies by Yamamoto et al. (1979), Finnigan and Einaudi (1981), and

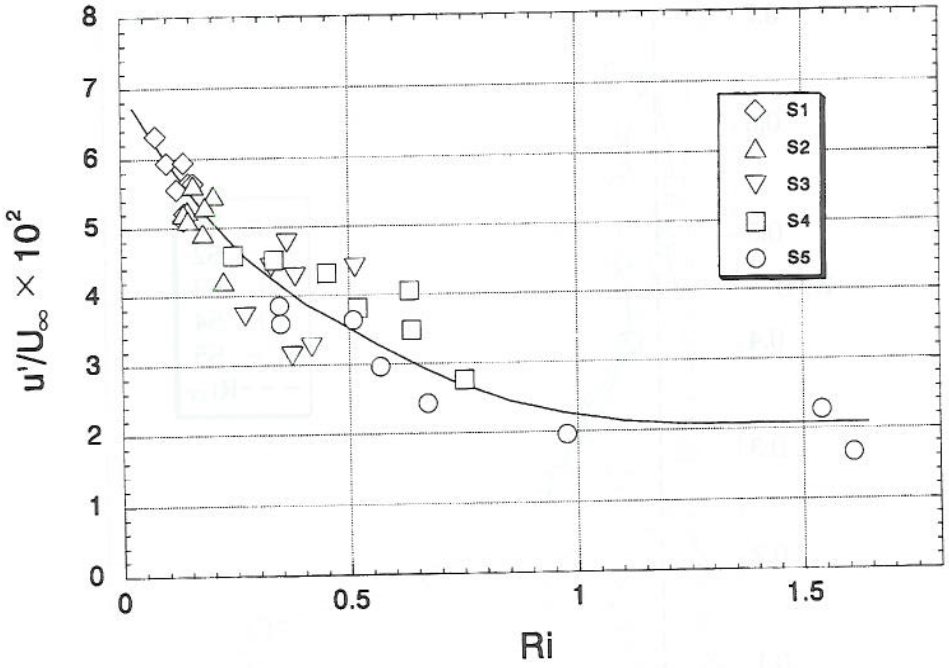

Figure 10a. Correlation of the turbulent intensity of u-component velocity u'/U_∞ with the local gradient Richardson number Ri.

Finnigan et al. (1984), showing a maximum at a certain height and approaching zero around the bottom and top of the boundary layer.

Figure 4b shows the vertical profiles of the vertical turbulent heat flux $\overline{w\theta}$. For this figure as well as Figures 3 and 4a, we can easily identify the two groups of the weak and strong stability cases. For the strong stability group (S3–S5), the heat fluxes $\overline{w\theta}$ are close to zero for $z/\delta < 0.2$. We can find similar profiles in the observational results from Finnigan et al. (1984) and Mahrt (1985), in which $\overline{w\theta}$ shows a maximum at a certain height, similar to the profile of momentum flux $\overline{uw}$. For the weak stability group (S1, S2), the $\overline{w\theta}$ variations in the vertical direction are similar to the results from Nieuwstadt (1984) and Mahrt et al. (1979) rather than those from Caughey et al. (1979), namely, $\overline{w\theta}$ decreases upwards almost linearly.

Figure 4c shows the vertical profiles of horizontal turbulent heat flux $\overline{u\theta}$. Also for this figure, the $\overline{u\theta}$ variations of the weak and strong stability groups show quite different profiles from each other. For the cases (S3, S4) of the strong stability group, however, the $\overline{u\theta}$ values never reach zero, but have some positive values for $z/\delta < 0.2$, different from the $\overline{w\theta}$ profiles. For the weak stability group (S1, S2), the $\overline{u\theta}$ rapidly decreases upwards.

Comparing the flux profiles shown in Figure 4 with the other experimental results in a wind tunnel, we can refer only to Arya (1975), as shown in Figure 4. The present flux profiles of $\overline{uw}$, $\overline{w\theta}$ and $\overline{u\theta}$ for the weak stability group (S1, S2:

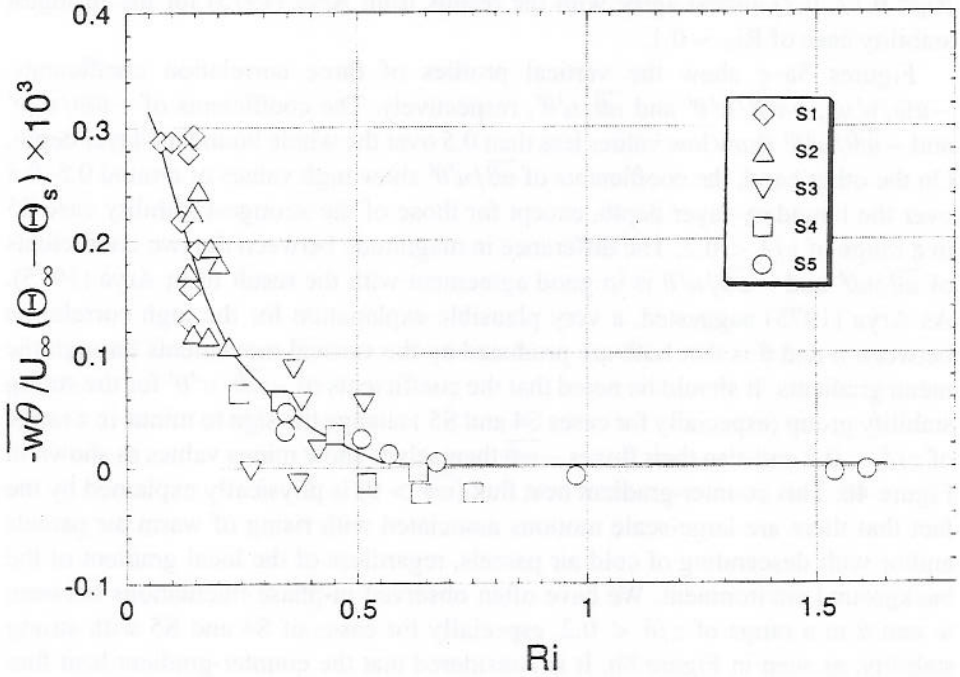

Figure 10b. Correlation of the vertical turbulent heat flux $-\overline{w\theta}$ with the local gradient Richardson number Ri.

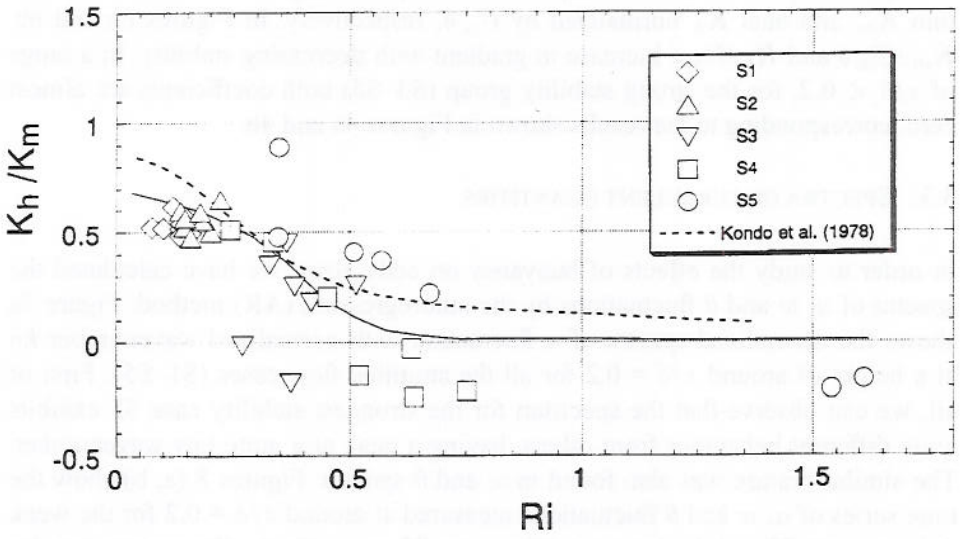

Figure 10c. Correlation of the ratio of heat and momentum eddy exchange coefficients K_h/K_m with the local gradient Richardson number Ri; solid lines are fitted curves; dashed line, the observational result from the Kondo et al. (1978).

Ri_δ= 0.12, 0.2) almost agree with the results from Arya (1975) for his strongest stability case of $Ri_\delta \sim 0.1$.

Figures 5a–c show the vertical profiles of three correlation coefficients, $-\overline{uw}/u'w'$, $-\overline{w\theta}/w'\theta'$ and $\overline{u\theta}/u'\theta'$, respectively. The coefficients of $-\overline{uw}/u'w'$ and $-\overline{w\theta}/w'\theta'$ show low values less than 0.5 over the whole boundary-layer depth. On the other hand, the coefficients of $\overline{u\theta}/u'\theta'$ show high values of around 0.5–0.8 over the boundary-layer depth, except for those of the strongest stability case S5 in a range of $z/\delta < 0.2$. The difference in magnitude between the two coefficients of $\overline{u\theta}/u\theta'$ and $-\overline{w\theta}/w'\theta$ is in good agreement with the result from Arya (1975). As Arya (1975) suggested, a very plausible explanation for the high correlation between u and θ is that both are produced by the vertical movements through the mean gradients. It should be noted that the coefficients of $-\overline{w\theta}/w'\theta'$ for the strong stability group (especially for cases S4 and S5) change the sign to minus in a range of $z/\delta < 0.2$ and also their fluxes $-\overline{w\theta}$ themselves show minus values as shown in Figure 4b. This counter-gradient heat flux ($\overline{w\theta} > 0$) is physically explained by the fact that there are large-scale motions associated with rising of warm air parcels and/or with descending of cold air parcels, regardless of the local gradient of the background environment. We have often observed in-phase fluctuations between w and θ in a range of $z/\delta < 0.2$, especially for cases of S4 and S5 with strong stability, as seen in Figure 8b. It is considered that the counter-gradient heat flux is due to the wave breaking such as internal gravity waves or due to the intermittent buoyancy-driven motions associated with the balance between potential and turbulent kinetic energies. However, the detailed feature remains unclear.

Figures 6a, b show the vertical profiles of eddy exchange coefficients of momentum K_m and heat K_h normalized by $U_\infty\delta$, respectively. In Figures 6a and 6b, $K_m/U_\infty\delta$ and $K_h/U_\infty\delta$ increase in gradient with decreasing stability. In a range of $z/\delta < 0.2$, for the strong stability group (S3–S5) both coefficients are almost zero, corresponding to the results shown in Figures 4a and 4b.

3.3. SPECTRA OF TURBULENT QUANTITIES

In order to study the effects of buoyancy on eddy sizes, we have calculated the spectra of u, w and θ fluctuations by the autoregression (AR) method. Figure 7a shows the normalized spectra of u fluctuation with normalized wavenumber $k\delta$ at a height of around z/δ = 0.2 for all the stratified flow cases (S1–S5). First of all, we can observe that the spectrum for the strongest stability case S5 exhibits quite different behaviour from others, having a peak at a quite low wavenumber. The similar feature was also found in w and θ spectra. Figures 8 (a, b) show the time series of u, w and θ fluctuations measured at around z/δ = 0.2 for the weak stability case S2 and the strong stability case S5, respectively. We can see that for the weak stability case S2 in Figure 8a, strong and high frequency turbulent motions dominate, whereas for the strong stability case S5 in Figure 8b, the small eddies corresponding to the high frequency fluctuations are greatly damped and low-

frequency fluctuations remain. Thus the flow in the lower part of boundary layer for the strong stability case S5 becomes very weak turbulence and is dominated by large-scale slowly fluctuating motions. Accordingly, the feature of spectrum of case S5 in Figure 7a reflects the quasi-laminar flow dominated by low-frequency fluctuations.

Figure 7b shows the normalized spectra of u fluctuation with $k\delta$ at five normalised heights for the case S2 with the weak stability group. Figure 7c also shows those spectra for case S4 with the strong stability group. For all the spectra of the weak stability flows as seen in Figure 7b, the peaks of spectra at five values of z/δ tend to shift gradually toward lower wavenumbers with increasing height. On the other hand, Figure 7c shows that, for the strong stability flows, the peak of spectrum at the lowest value of $z/\delta = 0.06$ occurs at a lower wavenumber compared with those at higher heights. This suggests a significant difference in structure in the lower part of boundary layers between the two stratified flows with weak and strong stability.

3.4. Vertical profiles of the local gradient Richardson number Ri

For the stratified flows as shown in Figures 3, 4, 7 and 8, we have noted that their turbulence characteristics are clearly divided into two groups of the weak and strong stability flows. To investigate the reason, we have considered the vertical profiles of local gradient Richardson number Ri for each stratified flow case in Figure 9. The straight broken line at a value of Ri = 0.25 in Figure 9 shows the critical Richardson number Ri_{cr} given by a linearized theory for inviscid flow. One notes that the two groups of stratified flows with weak and strong stability correspond to the two groups of the Ri profiles, separated by the Ri_{cr}.

3.5. Correlation of the turbulence quantities with the local gradient Richardson number Ri

As noted from Figure 9, it is expected that Ri is an important scaling parameter for correlating turbulent quantities. However, for the regions near the bottom and top of the boundary layer, both turbulent quantities and Ri greatly change in magnitude, as seen in Figures 3–6 and 9, suggesting a condition far from local equilibrium. Therefore, only values measured in a range of $0.1 < z/\delta < 0.5$ were adopted and correlated with Ri, as shown in Figure 10. In Figure 10, we have plotted three typical turbulent quantities from those shown in Figures 3–6 but correlated with Ri. Turbulence intensity u' rapidly decreases with increasing Ri, as shown in Figure 10a. Vertical turbulent heat flux $\overline{w\theta}$ also decreases with Ri and becomes almost zero with large Ri, as seen in Figure 10b. Figure 10c shows a variation of the ratio of the heat and momentum eddy exchange coefficients K_h/K_m. This variation with Ri is almost in agreement with the observational result from Kondo et al. (1978). Thus, the turbulent quantities in stable conditions are well correlated with Ri.

4. Conclusions

Using a thermally stratified wind tunnel, we have simulated various turbulent boundary layers under stable stratification conditions, which were fully developed over a long distance. To investigate the buoyancy effects on turbulent boundary layers, stable stratified flows with a wide range of stability (bulk Richardson number, Ri_δ, 0 to 1.33) were considered in the wind tunnel, while the Reynolds number, Re_δ, ranged from 3.14×10^4 to 1.27×10^5. The main results from the present study can be summarized as follows.

(1) Turbulent intensities of u and θ components as well as the w component are greatly suppressed with increasing stability.

(2) Momentum and heat fluxes for stratified flows are remarkably reduced by the stable stratification, compared with those for neutral flows. For the strong stability cases, the fluxes are almost zero in the lower part of boundary layers.

(3) According to the various vertical profiles of turbulence quantities, the boundary-layer flows are classified into three groups that consist of neutral flows, the stratified flows with weak stability (Ri_δ = 0.12, 0.2) and those with strong stability (Ri_δ = 0.39, 0.47, 1.33).

(4) The vertical profiles of turbulent intensities u', w' and θ' and turbulent fluxes $\overline{uw}$, $\overline{u\theta}$ and $\overline{w\theta}$ for the above three groups show similar distributions to the results from the corresponding observational studies.

(5) For the lowest part of boundary layers with strong and weak stability groups, those peaks of the u-, w- and θ-spectra exist at low and high wavenumbers, respectively. This suggests a difference in structure in the lower part of boundary layers between the two stratified flow groups with strong and weak stability.

(6) The two stratified flow groups with weak and strong stability exhibit quite different spectra and vertical profiles of turbulent intensities and fluxes from each other. This difference in turbulence characteristics clearly corresponds to the difference in the vertical distributions of local gradient Richardson number Ri , which are separated by the critical Richardson number $\mathrm{Ri}_{\mathrm{cr}}$.

(7) The lower part of stratified boundary-layer flows ($0.1 < z/\delta < 0.5$) is close to local equilibrium, and there the local gradient Richardson number Ri becomes a significant parameter for representing the buoyancy effects. Turbulence quantities in stable conditions are well correlated with Ri.

Acknowledgements

We should like to thank the referees for their helpful suggestions that have been incorporated in the final manuscript. Thanks are also due to Mr Boyajian of Engineering Research Center at Colorado State University for his assistance in the experiment and Mr A. Tanaka of the Interdisciplinary Graduate School of Engineering Sciences at Kyushu University for his help in the data analysis.

References

Andre, J. C. and Mahrt, L.: 1982, 'The Nocturnal Surface Inversion and Influence of Clear-Air Radiative Cooling', *J. Atmos. Sci.* **39**, 864–878.

Arya, S. P. S.: 1975, 'Buoyancy Effects in a Horizontal Flat-Plate Boundary Layer', *J. Fluid Mech.* **68**(2), 321–343.

Arya, S. P. S. and Plate, E. J.: 1969, 'Modeling of the Stably Stratified Atmospheric Boundary Layer', *J. Atmos. Sci.* **26**, 656–665.

Caughey, S. J.,Wyngaard, J. C., and Kaimal, J. C.: 1979, 'Turbulence in the Evolving Stable Boundary Layer', *J. Atmos. Sci.* **36**, 1041–1052.

Finnigan, J. J. and Einaudi, F.: 1981, 'The Interaction between an Internal Gravity Wave and the Planetary Boundary Layer. Part II: Effect of the wave on the turbulence structure', *Quart. J. Roy. Meteorol. Soc.* **107**, 807–832.

Finnigan, J. J. , Einaudi, F., and Fua, D.: 1984, 'The Interaction between an Internal Gravity Wave and Turbulence in Stably -Stratified Nocturnal Boundary Layer', *J. Atmos. Sci.* **41**, 2409–2436.

Garratt, J. R.: 1982, 'Observations in the Nocturnal Boundary Layer', *Boundary-Layer Meteorol.* **22**, 21–48.

Hunt, J. C. R., Kaimal, J. C., and Gaynor, J. E.: 1985, 'Some Observations of Turbulence Structure in Stable Layers', *Quart. J. Roy. Meteorol. Soc.* **111**, 793–815.

Komori, S., Ueda, H., Ogino, F., and Mizushima, T.: 1983, 'Turbulence Structure in Stably Stratified Open-channel Flows', *J. Fluid Mech.* **130**, 13–26.

Kondo, J., Kanechika, O., and Yasuda, N.: 1978, 'Heat and Momentum Transfers under Strong Stability in the Atmospheric Surface Layer', *J. Atmos. Sci.* **35**, 1012–1021.

Mahrt, L., Heald, R. C., Lenschow, D. H., Stankov, B. B., and Troen, IB.: 1979, 'An Observational Study of the Structure of the Nocturnal Boundary Layer', *Boundary-Layer Meteorol.* **17**, 249–264.

Mahrt, L.: 1985, 'Vertical Structure and Turbulence in the Very Stable Boundary Layer', *J. Atmos. Sci.* **42**, 2333–2349.

Meroney, N. R.: 1990, 'Fluid Dynamics of Flow over Hills/Mountains – Insights Obtained Through Physical Modeling', in W. Blumen (ed.), *Atmospheric Processes Over Complex Terrain*, American Meteorological Society, Meteorological Monographs **23**(45), 145–171.

Nicholl, C. I. H.: 1970, 'Some Dynamical Effects of Heat on a Turbulent Boundary Layer', *J. Fluid Mech.* **40**, 361–384.

Nieuwstadt, F. T. M.: 1984, 'The Turbulent Structure of the Stable, Nocturnal Boundary Layer', *J. Atmos. Sci.* **41**, 2202–2216.

Ogawa, Y., Diosey, P. G., Uehara, K., and Ueda, H.: 1982, 'Plume Behavior in Stratified Flows', *Res. Rep. Natl. Inst. Environ. Stud.* **33**, 29–60 (in Japanese).

Ogawa, Y., Diosey, P. G., Uehara, K., and Ueda, H.: 1985, 'Wind Tunnel Observation of Flow and Diffusion under Stable Stratification', *Atmos. Environ.* **19**(1), 65–74.

Piat, J.-F. and Hopfinger, E. J.: 1981, 'A Boundary Layer Topped by a Density Interface', *J. Fluid Mech.* **113**, 411–432.

Plate, E. J. and Cermak, J. E.: 1963, *Micrometeorological Wind Tunnel Facility: Description and Characteristics*, Fluids Dyn. & Diffusion Lab., Colorado State University, Rep. CER63EJP-JEC9.

Stull, R. B.: 1988, *An Introduction to Boundary Layer Meteorology*, Kluwer Academic Publishers, 666 pp.

Yamamoto, S., Yokoyama, O., and Gamo, M.: 1979, 'Observational Study of the Turbulent Structure of the Atmospheric Boundary Layer under Stable Conditions', *J. Meteorol. Soc. Japan* **57**, 423–430.